Toward Development of Improved QPE in Complex Terrain Using Cloud-to-Ground Lightning Data: A Case Study for the 2005 Monsoon in Southern Arizona

CARLOS MANUEL MINJAREZ-SOSA

Department of Atmospheric Sciences, The University of Arizona, Tucson, Arizona, and Departamento de Física, Universidad de Sonora, Hermosillo, Mexico

CHRISTOPHER L. CASTRO

Department of Atmospheric Sciences, The University of Arizona, Tucson, Arizona

KENNETH L. CUMMINS

Department of Atmospheric Sciences, The University of Arizona, and Vaisala, Inc., Tucson, Arizona

E. PHILIP KRIDER

Department of Atmospheric Sciences, The University of Arizona, Tucson, Arizona

JULIO WAISSMANN

Departamento de Matemáticas, Universidad de Sonora, Hermosillo, Mexico

(Manuscript received 17 September 2011, in final form 20 March 2012)

ABSTRACT

The relationship between convective precipitation and cloud-to-ground (CG) lightning is examined over a study area in southwest Arizona and northwest Mexico. Using seasonal-to-daily and hourly time resolution, the National Climatic Data Center (NCDC) stage IV precipitation product and the U.S. National Lightning Detection Network lightning data have been analyzed with the aim of developing an improved understanding of the relationship between these variables. A Gaussian method of spatially smoothing discrete lightning counts is used to estimate convective rainfall and improve the quality and spatial coverage of radar-derived precipitation in areas of complex terrain. For testing the dependence of the relationship between CG lightning and precipitation, a precipitation ''sensor coverage'' analysis has been performed. If locations that have poor sensor coverage are excluded, R^2 between lightning and precipitation improves by up to 15%. A complementary way to estimate convective precipitation is proposed based on 1-h lightning occurrence intervals, which is the maximum time resolution in this study. We find that ~67% of the seasonal 2005 precipitation over the analysis domain is associated with CG lightning. Daily precipitation estimates are improved by specifying a ''diurnal day'' based on the diurnal maxima and minima in precipitation and CG lightning within the domain. Our method for improving quantitative precipitation estimation (QPE) using lightning is able to track and estimate convective precipitation over regions that have poor sensor coverage, particularly in both air mass storms and large multicellular events, with R^2 up to 70%.

1. Introduction

Quantitative precipitation estimation (QPE) over a wide range of spatial scales has relevance for a variety of applications in climatology, hydrology, water resources,

Corresponding author address: Carlos Manuel Minjarez-Sosa, Department of Atmospheric Sciences, The University of Arizona, Physics and Atmospheric Sciences Bldg., Rm. 520, 1118 East Fourth Street, Tucson, AZ 85721-0081.
E-mail: minjarez@atmo.arizona.edu

DOI: 10.1175/JHM-D-11-0129.1

and agriculture (e.g., Grecu and Krajewski 2000; Todd et al. 2001; Krajewski and Smith 2002). On the continental-to-global scale, QPE can help characterize the lower-atmosphere energy budget and surface runoff (Sorooshian et al. 2005). On smaller space and time scales, QPE is a critical component in short-term forecasts (nowcasting) of flash floods, landslides, and other extreme weather events (e.g., Todd et al. 2001; Krajewski and Smith 2002). Rain gauges and weather radars are currently the standard datasets for observation-based QPE; however, each method has inherent weaknesses. Rain gauges provide an in situ measurement, but relatively poor spatial coverage, especially in remote areas where they are widely separated. Geostatistical methods employing gauges, terrain, and climatology may be used to improve areal QPE, the accuracy of which depends on season, accumulation period, and the density of stations [e.g., Parameter-elevation Regressions on Independent Slopes Model (PRISM); Daly et al. 1994]. Radar indirectly estimates areal QPE using a given reflectivity and rain rate (Z–R) relationship. While radar data can provide better spatial coverage than the rain gauges, its accuracy is affected principally by the presence of ice in the radar beam, evaporation of rain falling from relatively high altitudes (e.g., Crosson et al. 1996; Fulton 1999; Morin et al. 2005), and variation in the Z–R relationship (e.g., Foote 1966; Smith and Krajewski 1993; Morin et al. 2005).

It has been possible to combine both techniques and/or seek alternative methods and technologies in order to improve QPE (Stellman et al. 2001; Xie and Arkin 1995; Kursinski and Zeng 2006). Use of satellite data is one possibility that should be briefly mentioned. Satellite-derived precipitation estimates are not accurate at high space resolution (less than 0.5°) and the spatial coverage is limited by the satellite orbit (Anagnostou 2004). Since one of the goals of this research is to improve QPE on the mesoscale appropriate for characterization of thunderstorms, satellite data are unfortunately inadequate. Therefore we are practically limited to in situ precipitation gauge data and radar data for QPE. Considering both of these data sources, poor coverage in areas of complex topography is a problem since 1) most of the dense gauge networks are located in populated urban areas, not in rural mountainous regions and 2) there is terrain blockage of the radar beam. The terrain beam blockage issue has been described by Maddox et al. (2002) for operational National Weather Service radar sites, as shown in Fig. 1. Note that in the western United States the coverage is poor at 2 km AGL (Fig. 1a) and 1 km AGL is nonexistent over ⅔ of the landmass at Fig. 1b as compared to the central and eastern United States. The major U.S. cities in the intermountain west with populations greater than 1 million (Denver, Phoenix, Salt Lake City, Albuquerque, Tucson, Las Vegas, and El Paso) are all located near mountain ranges where terrain beam blockage is a problem. In the Tucson weather forecast office (WFO), lightning information is used in a subjective way to locate convective storms and compensate for terrain blockage, but not for quantitative estimation of rainfall rates. In this study, we consider the southern Arizona area that includes Tucson (Fig. 2) located in a basin and surrounded by mountains of varying elevation on all sides.

Can lightning data possibly augment the QPE for convective rainfall in areas of complex terrain? We proceed on the premise that the answer is affirmative and if so, this may potentially improve short-term QPE in the western United States (e.g., nowcasts of flash flooding). A statistically significant relationship between cloud-to-ground (CG) lightning and convective precipitation is physically explained by the fact that the cloud electrification process requires supercooled water, ice particles, and larger, heavier graupel to coexist in a region experiencing moderately high updraft velocities (Takahashi 1990; Petersen and Rutledge 1998). Lightning is thus invariably accompanied by precipitation during most of the life cycle of a lightning-producing cell (e.g., Battan 1965; Petersen and Rutledge 1998; Gungle and Krider 2006).

Decades of observational evidence (e.g., Lhermitte and Krehbiel 1979; MacGorman et al. 1989; Wiens et al. 2005; Latham et al. 2007; MacGorman et al. 2008) and recent modeling studies (e.g., Baker et al. 1995; Latham et al. 2004; Mansell et al. 2005) have established that the rate of all lightning discharges (i.e., intracloud discharges plus cloud-to-ground flashes) is strongly correlated with the rate of cloud electrification, and that the latter is controlled by the convective cycles, the updraft mass flux, and the mass of ice-phase precipitation. Also, Reap and MacGorman (1989) and MacGorman et al. (2008) have suggested that the rates of CG flashes are typically not correlated with the storm severity or the updraft intensity, but rather are correlated with the formation of precipitation and its descent to lower levels of the storm.

In general, prior work (e.g., Battan 1965; Petersen and Rutledge 1998; Gungle and Krider 2006) has shown that a strong but somewhat variable statistical relationship exists, likely suitable for operational forecast application of a lightning-augmented QPE. This correlation between lightning and precipitation, with respect to temporal and spatial resolution, has not yet been explored in depth. The work presented here is one of the first studies that compares cloud-to-ground lightning with ground level multisensor precipitation. We diagnostically assess the lightning–precipitation relationship for a given event and over a single season in order to show efficacy in the intermountain west. The paper is

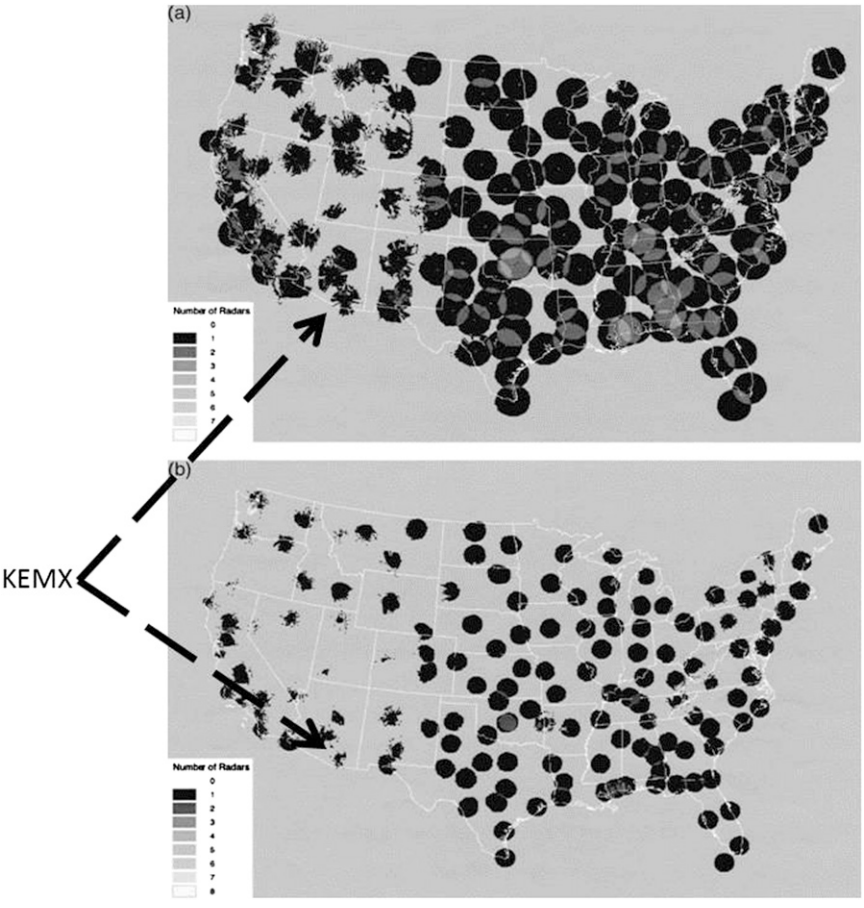

FIG. 1. Coverage of the Weather Surveillance Radar-1988 Doppler (WSR-88D) network at heights of (a) 2 and (b) 1 km AGL (from Maddox et al. 2002). The location of the Tucson NEXRAD radar (KEMX) is indicated by arrows.

organized as follows: in section 2, the research area and data are discussed; section 3 describes the methodology employed in the study; then, section 4 shows the results for the 2005 season, including hourly, daily, and diurnal analysis along with a storm case study. Section 5 presents discussion and conclusions and planned future work.

2. Research area and data

a. Spatial domain and general meteorological conditions

The Next Generation Weather Radar (NEXRAD) radar site (KEMX) for the study is located near Tucson, Arizona, and provides varying quality coverage in the study area enclosed by 30.914°–32.4566°N latitude and −109.731°–111.445°W longitude. In this initial demonstration study of our methods, we analyze only the 2005 summer [June–August (JJA)] season. This region receives about half of its annual precipitation during the North American monsoon in late summer (Douglas et al. 1993; Adams and Comrie 1997). Average precipitation during the summer months is approximately 150 mm, per the climatological record of the Tucson weather service forecast office (WSFO). Monsoon convective precipitation requires deep lower-tropospheric moisture and elevated topography for initiation of thunderstorms (Zehnder et al. 2008; Adams and Souza 2009). Convective clouds build over the high terrain, beginning in the late morning or early afternoon, driven by the diurnal mountain–valley circulations. In Tucson, these are mainly the highest mountains to the north and east of the city—the Catalinas and the Rincons, respectively. Most of the convective precipitation occurs in the mountains and less at lower elevations (e.g., Castro et al. 2007). Depending on the large-scale environment (e.g., Maddox et al. 1995), monsoon thunderstorms may grow and propagate off the terrain in late afternoon and/or trigger the development of (typically) new thunderstorms in lower elevations by outflow boundaries (e.g., Smith and Gall 1989). Though typically not as strong as

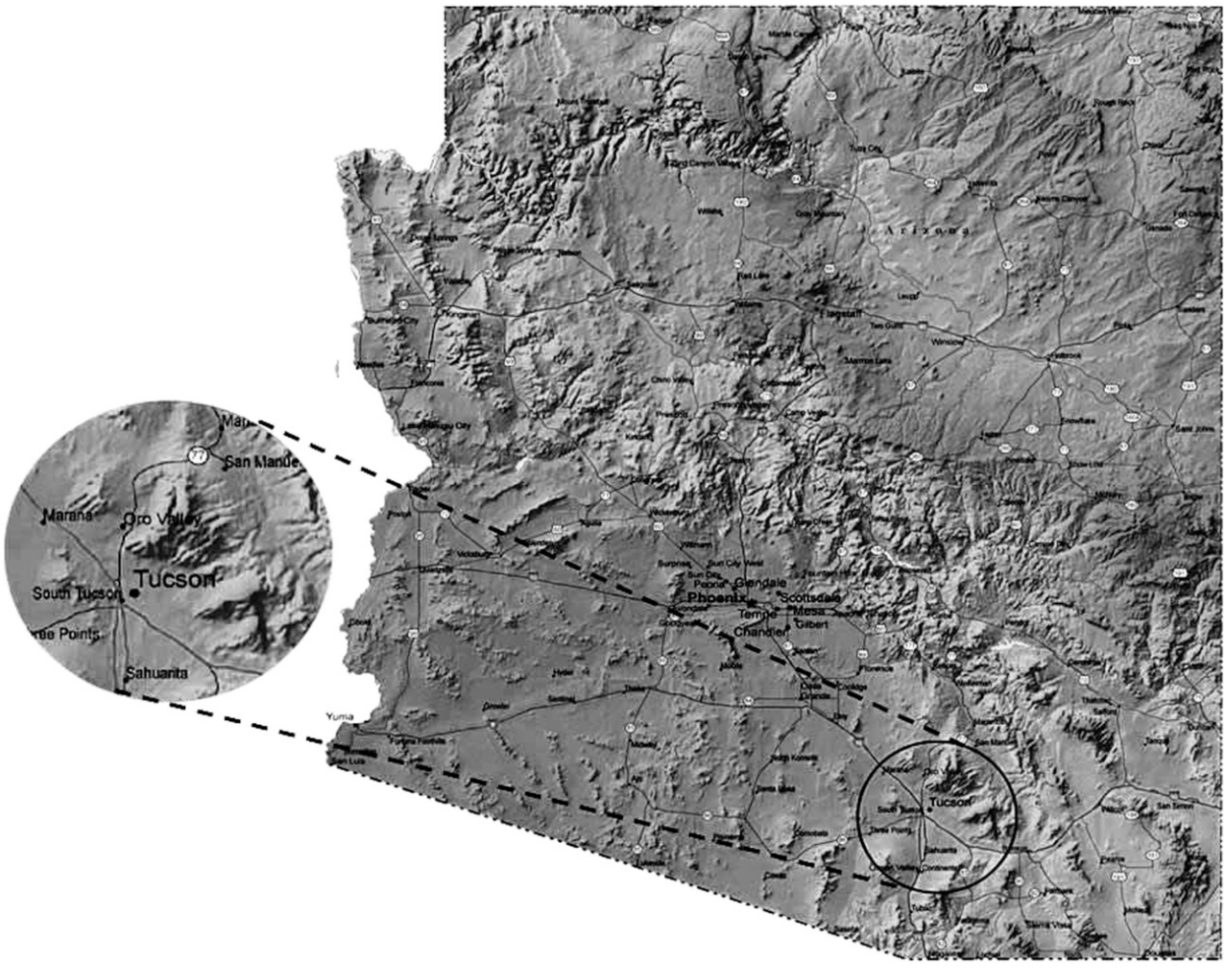

FIG. 2. Southern Arizona topography and roads. Inset provides an expanded view of the Tucson basin. Note that there are mountains in all directions around Tucson.

their counterparts in the central United States, mesoscale convective systems (MCSs) in Arizona during the monsoon have the same salient characteristics, with leading lines of heavy precipitation followed by a much larger area of light and steady precipitation in a trailing stratiform region (e.g., Houze et al. 1990). Because of the presence of substantial stratiform precipitation, consideration of MCSs poses a challenge for developing a single method for incorporating lightning data in QPE, as will be discussed in section 6.

As previously mentioned in the introduction, QPE in the Tucson region is substantially affected by radar beam blockage. The majority of the precipitation that occurs over the surrounding mountains cannot be measured by radar alone. For example, Fig. 3 (next subsection) shows the Hydrometeorological Automated Data System (HADS) and the Tucson Automated Local Evaluation in Real Time (ALERT) rain gauge networks (black asterisks) that contribute to the stage IV (ST4) dataset and the coverage of the KEMX radar station. The white regions do not have sensor coverage based on our criteria (discussed later). Coincidentally, the areas of beam blockage also have very sparse rain gauge coverage (particularly to the southwest of the KEMX radar), because most of the gauges are located within the Tucson metropolitan area. The coverage shown in Fig. 3 reflects approximate density of the gauge network, since not all HADS sites are operational, and additional gauges could be used in some locations.

b. Precipitation data

The NCEP ST4 precipitation dataset is a U.S. national multisensor analysis that is built from the regional multisensor analyses of 12 conterminous United States (CONUS) River Forecast Centers (RFCs; Lin and Mitchell 2005). Every RFC produces its own analysis using the algorithm proposed by Fulton et al. 1998 and Fulton (1999) for multisensor data and employs some

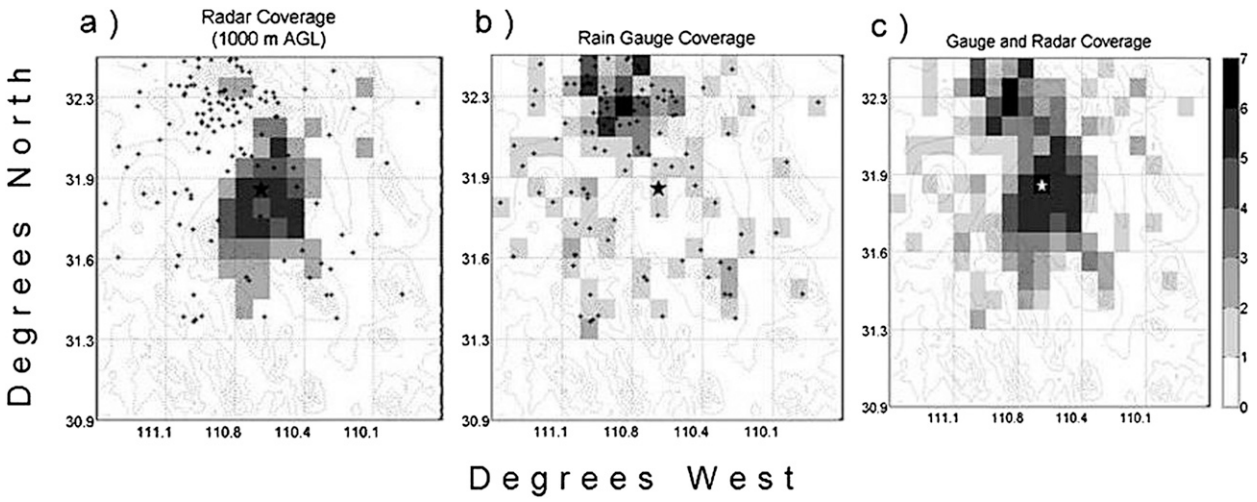

FIG. 3. Steps for producing coverage analysis for the ST4 grids (black asterisks indicate the gauge location; black star indicates the KEMX radar location): (a) count of radar tilts below 1000 m AGL; (b) number of rain gauges per grid; and (c) union of (a) and (b)—for this case, white star is the KEMX radar location.

manual quality control (Lin and Mitchell 2005). Each RFC carries out their analysis using the corresponding NEXRAD Weather Surveillance Radar station(s) and the HRAD rain gauges in their domain at two time resolutions: 1 and 6 h. Subsequently, NCEP produces a national ''composite'' (mosaic) dataset with the same time resolutions, as described by Lin and Mitchell (2005). The final national products are 4 km space resolution polar stereographic grids every 1 or 6 h for the whole continental United States and surrounding areas (for this study we converted to an 8-km latitude–longitude grid).

c. *Lightning data*

The CG lightning data have been provided by the U.S. National Lightning Detection Network (NLDN). This network consists of about 113 Improved Performance from Combined Technology (IMPACT) sensing antennas located throughout the continental United States (Cummins and Murphy 2009). The typical separation between sensors is roughly 300 km, and a single lightning discharge is typically seen by six or more sensors. Combining two parameters from each sensor (time of arrival and magnetic direction), the NLDN provides the flash locations with median location accuracy of ~0.5 km and a time accuracy of ~1 μs (Cummins et al. 1998; Cummins and Murphy 2009). According to Biagi et al. (2007), the NLDN detects over 90% of the CG flashes in southern Arizona and it is a particularly useful tool for this study.

d. *Topography data*

Topography data were utilized to analyze radar the spatial coverage provided by the KEMX NEXTRAD radar. The Digital Terrain Elevation Data (DTED) developed by the National Imagery and Mapping Agency (NIMA) was used as the digital elevation model (DEM). For DTED, the elevation is given in meters above mean sea level (MSL). Its accuracy is ±50 m in the horizontal and ±30 m in the vertical. The horizontal latitude–longitude resolution is 30 arc seconds (~1000 m).

3. Methodology

a. *Correlation analysis*

There is a demonstrated relationship between convective precipitation and CG lightning (e.g., Battan 1965; Petersen and Rutledge 1998; Gungle and Krider 2006). At higher time and space resolutions, studies have shown that lightning events are located in the vicinity of elevated, high-reflectivity radar echoes where high precipitation volumes occur during short time intervals (Reap and MacGorman 1989; Tapia et al. 1998). For this study, hourly ST4 precipitation data have been interpolated from polar stereographic coordinates onto a geographic latitude–longitude grid with a 8-km grid mesh and are represented here as the variable P. Then, NLDN lightning first strokes (CG flashes) are accumulated over the same space and time resolution as ST4 data for the months of June, July, and August 2005. For some of the analysis, ''smoothed'' lightning counts are employed, as described in the following subsection (3b). Finally, a criterion to separate the precipitation explained by lightning (PEL) and the precipitation not explained by lightning (PNEL) has been applied. The methodology employed for separating the types of precipitation is explained in subsection 3d.

With regards to the underlying relationship between CG lightning and convective rainfall, some studies have shown a significant correlation employing a linear relationship (Piepgrass et al. 1982; Petersen and Rutledge 1998; Gungle and Krider 2006; among others), while some others have preferred a power-law relationship (e.g., Battan 1965; Cheze and Sauvageot 1997; Saylor et al. 2005). Theoretical work by Latham et al. (2004) indicates that the power-law exponent should depend on the glaciation mechanism. When glaciation is produced by primary nucleation, this relationship is theoretically linear (exponent = 1). Saylor et al. (2005) carried out a survey of these different methodologies and found that those studies that used a linear relationship to correlate ''bulk'' parameters like rain rate, rain mass, or rain volume showed high variability in the relationship (rain yields) from storm to storm. They argued that it is more useful to include the dependence of lightning on the drop size distribution (Fher et al. 2005; Soula and Chauzy 2001; among others). Additionally, several studies have shown that flash polarity has a role in the relationship under conditions where a fraction of flashes have positive polarity. As will be discussed in section 4, for our domain, a linear relationship shows statistical significance with no dominant nonlinearity. Therefore, it was not necessary to use a more complicated power-law relationship. Additionally, no more than 1% of the CG flashes for the analyzed MCSs were found to be positive for this study, hence we only consider the total number of CG flashes, regardless of the polarity.

For this study, regression analysis between P and L has been carried out in two ways. First we compared the precipitation per grid $P_{i,j}$ for a given period of time (where i and j represent the grid latitude–longitude position) with the number of CG lightning flashes for the same grid $L_{i,j}$. In this case, the number of points in the regression is equal to the number of grids (with lightning) in the analysis domain. The other approach was to relate the total amount of precipitation $P(t)$ within the 23 000-km^2 domain area, as a function of time, with the total number of CG lightning flashes $L(t)$; in this case, the number of points in the regression equals the number of time steps (with lightning) over the analysis interval. Then, the statistical significance of the correlation coefficient is evaluated through a Student's t test.

b. Gaussian convolution

A simple linear regression between precipitation and lightning can be used to determine the ''precipitation yield'' (mm flash^{-1} or m^3 flash^{-1}). However, precipitation and CG lightning flash counts are continuous and discrete variables, respectively. A precipitating convective cell can show regions with intense precipitation and this pattern generally decays outward from the convective core in a continuous way, particularly if the precipitation is derived from a Z–R relationship. On the other hand, lightning flashes occur discretely and therefore maps of short-term lightning count fields are spatially discontinuous. However, other studies have shown that CG flashes frequently have multiple ground contacts. For instance, Stall et al. (2009) reported more than 50% of multistrokes negative CG flashes have multiple ground contacts, and the mean separation between the ground contacts for southern Arizona was about 2.6 km. This spatial ''spread'' of a CG flash, coupled with the inherent errors in the lightning locations, supports obtaining a more spatially continuous representation of CG lightning strikes as described below.

Instead of representing a CG flash at a single-point location, lightning occurrences are convolved with a two-dimensional Gaussian distribution and integrated to the 8-km ST4 grid. Figure 4 visually illustrates these steps. Figure 4a shows the individual first-strokes locations (white dots), superimposed on the Gaussian lightning count distribution at 0.5-km resolution, and Fig. 4b shows the same distribution on the coarser ST4 grid.

c. Gauge and radar coverage

There are two important considerations for the area covered by radar: 1) terrain blockage of the radar beam and/or 2) a radar beam that is too high above ground level (AGL) to accurately represent precipitation on the ground. The latter consideration takes into account suggestions by our colleague Dr. Robert Maddox—an expert in both radar meteorology and severe weather—who provided consultation on this work. Dr. Maddox suggested that radar-derived precipitation should be considered within only 50 km of the radar site. To ensure reliable radar precipitation estimates, only pixels for which at least one radar beam angle comes within 1 km of the surface are considered as ''covered.'' This is even a less restrictive criteria than that suggested by Dr. Maddox. The total radar coverage (TRC) is the matrix resulting from the addition of coverage matrices for the five lowest radar tilts, each with values of either 0 (not covered) or 1 (covered). The TRC matrix is upscaled using a nearest-neighbor method averaging to the spatial resolution of ST4 precipitation data. For radar, if we have TRC > 1 (at least two tilts below 1000 m AGL), then this grid is considered covered.

The rain gauge coverage (RGC) matrix is simpler than the TRC. A grid is considered covered if it contains at least one gauge. The total coverage is given by the union of the grids covered by radar and rain gauges. Figure 3 visually shows the steps of the coverage analysis.

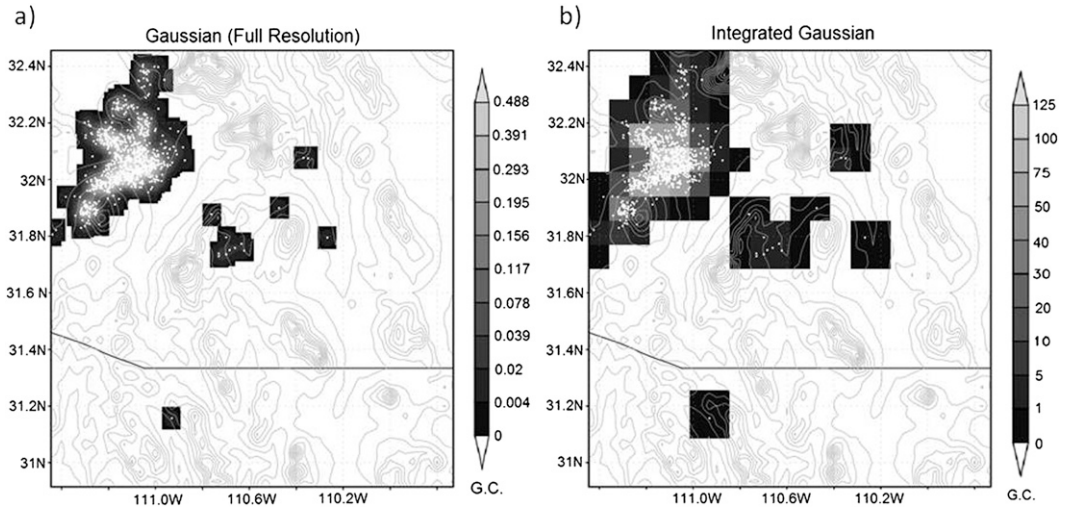

FIG. 4. Gaussian spatial smoothing of lightning flashes. (a) Gaussian convolution of flash locations (white dots); (b) Gaussian data integrated to the ST4 spatial resolution. [scale bar in Gaussian counts (G.C.).]

By the end of the process, only ~30% (109/360) of the total grids in the domain are considered to have good coverage. Note that the grid points with coverage are located either very near the radar site itself (black star; white star in 3c), in the region with multiple radar tilts, or at rain gauge sites at relatively low elevations off the peaks of the terrain.

The procedure described above is an approximation to the digital hybrid scan terrain compensation method used in stage IV because 1) the actual process includes several radars, 2) owing to occasional failure the number of rain gauge stations may change for some time periods, 3) there may be other gauges that are not included, and 4) our AGL height requirement is quite strict. Since most supplementary stations are close to the city, this ''good coverage'' approximation should still be appropriate under most conditions.

d. Seasonal, daily, and diurnal analyses

Before considering how lightning-derived precipitation ($\hat{P}$) can help improve QPE of individual rainfall events, it is necessary to evaluate the lightning–precipitation relationship (LPR) on seasonal and daily bases to see if our results compare favorably with previous studies in Arizona by Petersen and Rutledge (1998) and Battan (1965). A problem that arises therein, however, is how to differentiate between convective and nonconvective (typically stratiform) rainfall. Several criteria have been previously used to assess this, contingent on the given QPE method. Gungle and Krider (2006) defined convective precipitation by a rain rate threshold measured by a rain gauge network and the number of gauges that exceed the threshold, while Petersen and Rutledge (1998) used a combination of climatological and meteorological criteria to determine the threshold of convective and nonconvective precipitation. In this study, we simply consider precipitation statistically explained by lightning (PEL) and precipitation not statistically explained by lightning (PNEL), assuming that the former is due primarily to convective precipitation and the latter comprises mostly stratiform and warm convective precipitation. PEL is defined to be precipitation in grids that also contain at least one CG flash per hour (the highest time resolution used in ST4 dataset) or >0.25 for Gaussian integrated CG counts. In terms of representing the precipitation of propagating monsoon thunderstorms in Arizona, this classification method will only provide an improved QPE for isolated of air mass thunderstorms or leading squall lines of organized convection. The lightning-derived precipitation $\hat{P}$ will probably not provide a good lightning-derived estimate in areas of trailing stratiform precipitation, and we discuss potential ways to address this problem in section 5.

The time used in this study is coordinated universal time (UTC) throughout Arizona where 0000 UTC is 1700 local standard time (LST). Several studies have shown that there is a maximum in monsoon precipitation at about 1400 LST over the high terrain while over the lower terrain this maximum is about 1700 (Balling and Brazel 1987; Becker and Berbery 2008; Li et al. 2008). Other studies have shown that there can be time lags from 0 to 45 min between precipitation and CG lightning in convective events (e.g., Rutledge and MacGorman 1988; Soula and Chauzy 2001; Gungle and Krider 2006). When day boundaries are based on UTC time, the maximum precipitation and maximum in CG

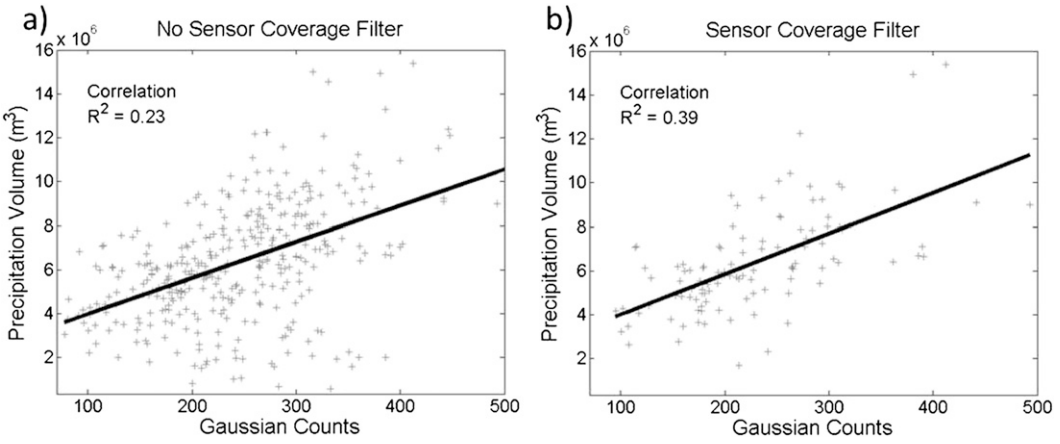

FIG. 5. Scatterplots for the gridded seasonal (JJA) ST4 precipitation volume (m^3) ''explained by lightning'' (PEL) vs CG flash counts: a) ''no sensor filter'' and b) ''with sensor filter'' (see text for details).

events can be ''lagged'' by what appears to be 1 day (before and after 1700 LST), due solely to the temporal distribution of convection in the region. Thus, to facilitate matching of precipitation and CG lightning data, we start the analysis at the time of minimum precipitation, as detailed in section 4d.

4. Results

During the 2005 summer, there were 63 events with precipitation (at least some) within the domain, 10 of which had significant precipitation ($>2 \times 10^7$ m^3) accumulated over our domain (see Fig. 7). As will be shown in section 4c, more than 50% of the precipitation within these events was explained by lightning.

a. Sensor coverage effect on the LPR

Figure 5 illustrates the effect of the radar and gauge coverage problem in the ST4 dataset and its impact on the LPR. This image compares the scattergrams for two cases: no sensor coverage filter (Fig. 5a) and with a sensor coverage filter (Fig. 5b). Results of the regressions are listed in Table 1. Each data point represents the seasonal accumulation of precipitation and the Gaussian lightning counts at the selected 109 grid points. If no coverage filter is applied, the correlation is statistically significant (99.9% of statistical significance) with a relatively low $R = 0.48$. If the coverage filter is applied, and only points with ''good'' radar and rain gauge coverage are included, as indicated by the colored regions in Fig. 3c, then R improves to 0.62. For this reason, subsequent correlation and regression analyses will only employ filtered data.

Figure 5 shows a notable nonzero intercept in the regression, even using just PEL, which excludes grids with no lightning. This behavior is due to the nature of the regression. When a spatial regression (over grids) is calculated, the method does not consider the following factors: 1) the difference in precipitation yield that can exist because of the topography, and 2) the variety of convective events over the analyzed period that occurred in different regions. So, in general, this regression tries to accommodate variations in the relationship over the entire spatial domain and over all convective events. The time resolution of the ST4 product affects the correlation as well. Within 1 h a single grid area can experience both convective and stratiform precipitation as the storm develops and decays, so the temporal resolution is insufficient to resolve this difference.

b. Precipitation and CG lightning relationship: Summer 2005 spatial analysis (JJA)

ST4 QPE is affected by the low area density of rain gauges and by radar beam blockage into the Tucson area. Figure 6 shows a sequence of images where the problem is illustrated in the 2005 summer season (JJA). This figure also illustrates the basic procedure for constructing $\hat{P}$ using Gaussian-derived flash counts. Figure 6a shows the multisensor ST4 PEL over the whole

TABLE 1. Regression parameters from Fig. 5. First column is precipitation volume per CG flash (m).

m (m^3 $flash^{-1}$)	y intercept (m^3)	R	R^2
Case (a) precipitation volume vs integrated Gaussian (no sensor filtered)			
16 408	2 353 706	0.48	0.23
Case (b) precipitation volume vs integrated Gaussian (sensor filtered)			
18 436	2 169 638	0.62	0.39

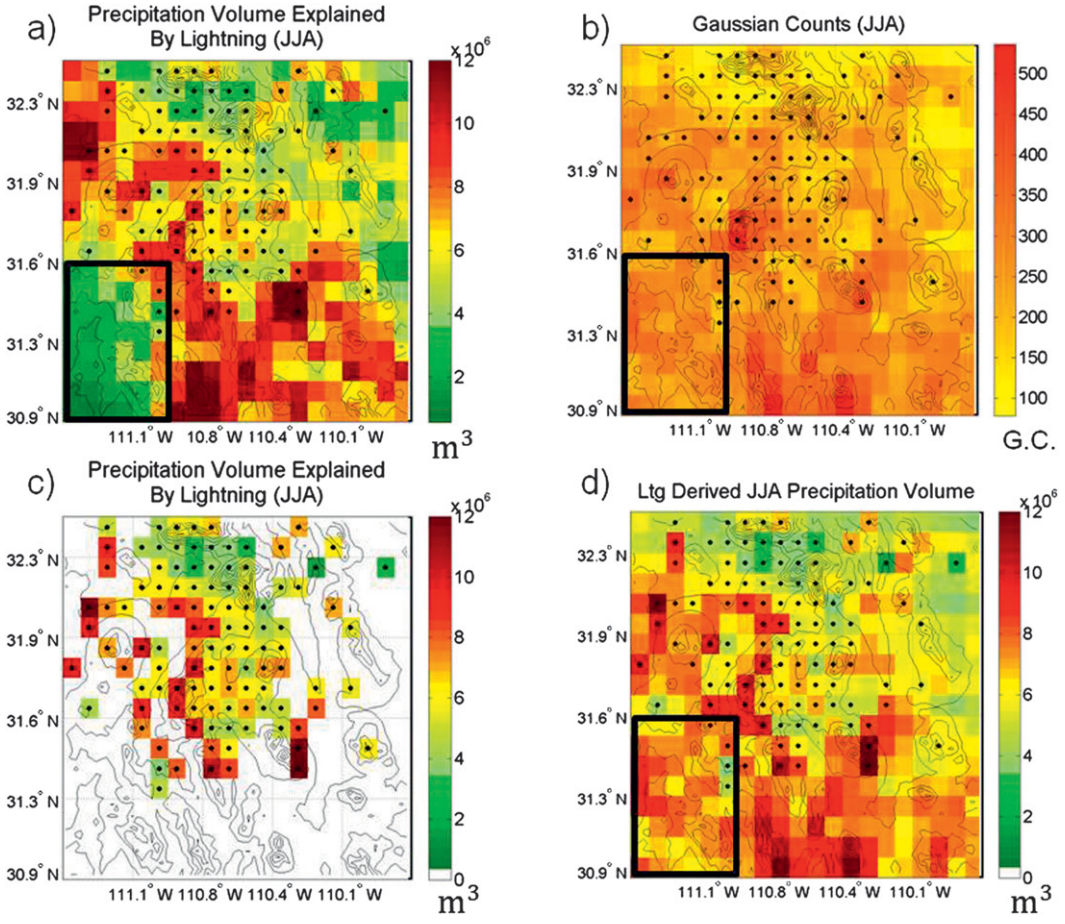

FIG. 6. Procedure for constructing lightning-derived precipitation: (a) accumulated PEL (m^3)—dots show grids with sensor coverage; (b) integrated Gaussian CG flash counts; (c) as in (a), but only for the covered regions; (d) final lightning-derived precipitation (just for nonsensor-covered grids, after applying regression in Fig. 5b) (Table 1). Black rectangle in southwest corner shows the impact of beam blockage on ST4 precipitation and the resulting improvement when using CG lightning information.

domain, and Fig. 6c shows only the grids that have good sensor coverage. The corresponding seasonal CG flashes are shown in Fig. 6b. The associated $\hat{P}$ (Fig. 6d) employs the lightning data for the grids with no sensor coverage (the sensor-covered grids have the same values than Fig. 6a). In Fig. 6d, the relationship of 1.8×10^4 m^3 $flash^{-1}$ plus 2.1×10^6 m^3 obtained from the linear regression (Gaussian) is used for lightning-derived rainfall (see Table 1).

Comparing Figs. 6a and 6d, there is generally good agreement between PEL and the composite precipitation $\hat{P}$ throughout much of the noncovered domain. On the other hand, it is also clear how the southwest zone of ST4 precipitation (enclosed by the black rectangle in Fig. 6) is affected by radar beam blockage. This area is on the Tohono O'odham Nation, which only has rain gauge coverage in the northeast (NE) corner of the rectangle, so the ST4 dataset is based only on very high-altitude (AGL) radar observations and/or spatial interpolations of rain gauge measurements. The same is also true for the southern part of the region extending into northern Mexico. For this region, the lowest radar tilt is >2.5 km AGL so it is impossible to know if moisture associated with the elevated echo actually reaches the ground. Knowledge of $\hat{P}$ may be of great help in such places. The northwest corner of the study region shows higher ST4 PEL (Fig. 6a) than is estimated by lightning (Fig. 6d); this may be due to stratiform precipitation, which is not well correlated with lightning, as this is a relatively more lowland desert area away from the mountains.

c. *Summer 2005 temporal analysis (24-h time resolution)*

The discrete lightning counts and Gaussian integrated lightning counts were accumulated in a daily UTC day for JJA 2005, and correlated with the corresponding

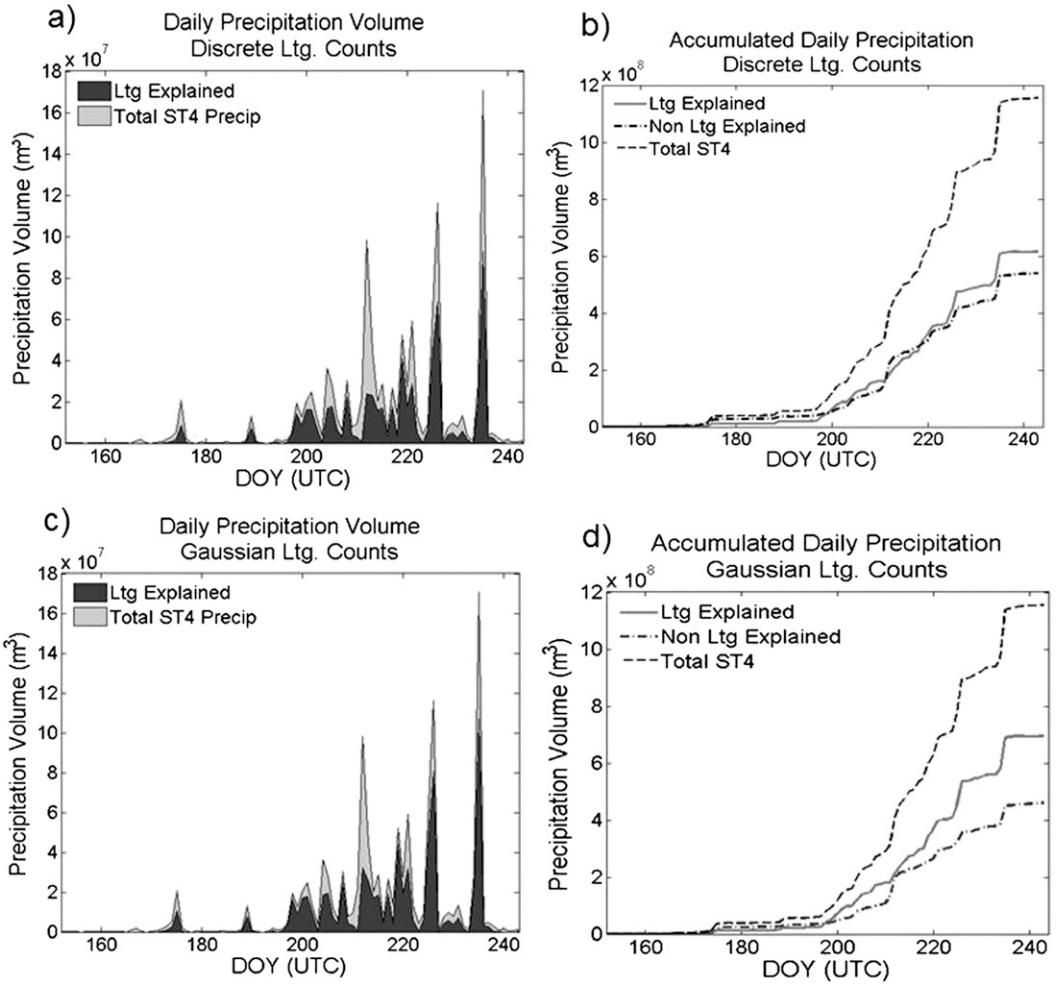

FIG. 7. Daily (UTC) analysis of precipitation volume for JJA 2005. (a),(c) Daily total volume from ST4 and PEL fractions. (b),(d) Seasonal accumulations of total, PEL, and non-PEL precipitation. Discrete lightning counts are employed in (a) and (b); Gaussian counts are employed in (c) and (d).

daily accumulation of the precipitation volume. The method used to separate PEL and PNEL provides a rough approximation of convective and stratiform precipitation, respectively. The stacked plots in Figs. 7a and 7c show comparisons of daily time series between both types of precipitation with discrete CG counts and integrated Gaussian counts, respectively. The Gaussian integrated lightning counts explain more of the precipitation volume (67%) than the discrete CG counts (52%) (see Figs. 7b,d) because of the spatial smoothing, which spreads the CG lightning counts to more grids, thereby classifying a larger fraction of the precipitation as PEL than the discrete CG counts. The linear regression of both CG discrete counts and Gaussian integrated counts with ST4 daily precipitation are both statistically significant at the 99% level (see Figs. 8a,b). For these regressions, each point represents precipitation and lightning integrated over the whole spatial domain. The slightly lower correlation obtained using the integrated Gaussian may be due to the large (8×8 km) grids with hourly data; that is, if as few as one CG flash smoothed into a nearby grid cell, all the precipitation in that grid is counted in the correlation analysis, and hence this method could partially include stratiform precipitation. The two outliers that are seen in the scattergrams will be discussed further below.

The seasonal precipitation volume per flash (PVF; m^3 $flash^{-1}$) obtained from regression analysis is shown in Table 2, calculated excluding the outliers noted above. For this study, the ratios obtained using discrete count and Gaussian counts (GC) were $\sim 1.7 \times 10^4$ m^3 $flash^{-1}$ and $\sim 1.8 \times 10^4$ m^3 $flash^{-1}$, respectively. The differences in all PVF values are ~10%, and may not be significant given the small degree of freedom in the regressions. There are very few published studies for southern Arizona that relate precipitation and CG lightning. Battan

TABLE 2. Regression parameters from Figs. 8a,b.

m (m^3 $flash^{-1}$)	y intercept (m^3)	R	R^2
Case (a) precipitation volume vs lightning counts			
17 000	1 509 200	0.82	0.67
Case (b) precipitation volume vs integrated Gaussian			
18 300	1 962 200	0.80	0.64

(1965) observed 29 individual storms and found an average precipitation yield of 3–6 $\times$ 10^7 kg $flash^{-1}$ (with a power law), equivalent to a PVF of 3–6 $\times$ 10^4 m^3 $flash^{-1}$ (gauge estimation and visual lightning counts). Petersen and Rutledge (1998) obtained a precipitation yield of 5.7 $\times$ 10^7 kg $flash^{-1}$ (5.7 $\times$ 10^4 m^3 $flash^{-1}$) in the southwest United States. These values are somewhat larger than the storm-average PVF for CG flashes in Florida thunderstorms (2.6 $\times$ 10^4 m^3 $flash^{-1}$) found by Gungle and Krider (2006). Overall, the precipitation yield (and PVF) obtained in this study are of the same order as those obtained by other authors for the same geographical area. Differences in precipitation yield obtained for the three studies in southern Arizona (including this one), are likely due to different convective/stratiform classification methods, the different sources of precipitation and lightning data, and natural variability.

Focusing on the regression analysis in Figs. 8a and 8b, it is clear that there are two different behaviors in the scattergrams—those points near and below the regression line that resemble the average behavior over the season—and those substantially above the regression lines that are extraordinary events (pointed by arrows). The former mostly correspond to the normal monsoon air mass thunderstorms; the later correspond to MCSs that occurred on 14 and 23 August. For these two cases, much of the precipitation occurred in large trailing stratiform regions that exhibit very low lightning rates. This behavior will naturally result in higher rain yields. The event that occurred on 14 August will be examined further in section 4e.

To address the stability of the linear regression, two analyses were carried out. First, we employed robust regression with a bisquare weighting function and 4.685 tuning constant, after excluding the two ''outlier'' events in August. The resulting RMSE was decreased by 2.5%. We also evaluated a power-law relationship of the form $y = ax^k$ (results not shown). The power-law relationship increased the MSE, primarily because it was not able to address the large nonzero intercept in these relationships. Therefore, considering at least our data, a linear regression is sufficient to relate CG lightning and convective precipitation. When comparing these results to the seasonal spatial correlation in section 4a, these daily values exhibits a much smaller intercept. Additionally, the correlations for lightning counts and Gaussian counts (Table 2b) are much higher than their counterparts in Table 1. The improved results in this section may be due to the fact that this daily temporal analysis averages over the whole sensor-covered domain, thus ''averaging out'' the influence of spatial (topography) variations.

d. Diurnal analysis

As discussed at the end of section 3d, the use of the ''UTC day'' for daily evaluation can increase the uncertainty in the relationship because of a time lag

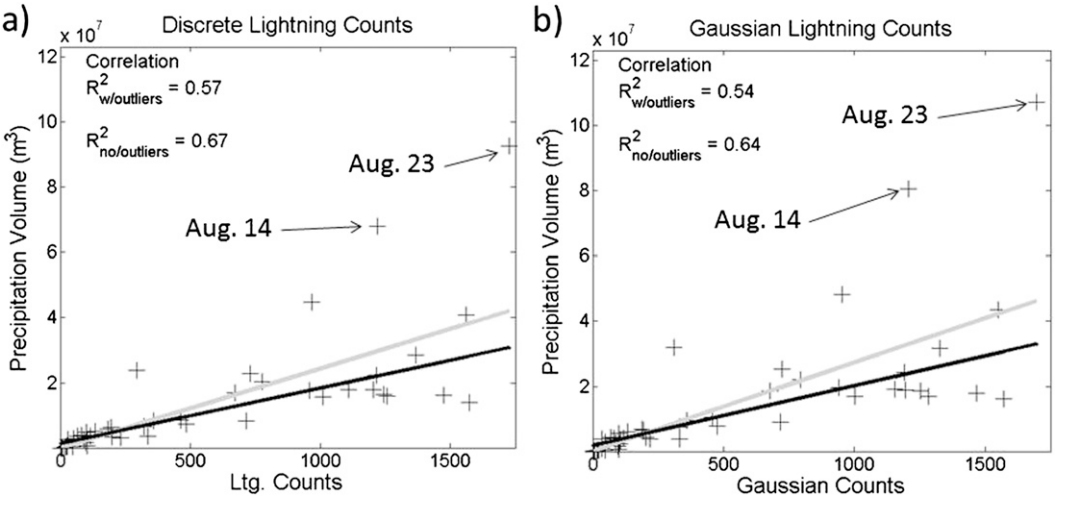

FIG. 8. Scattergrams of daily ST4 PEL vs (a) discrete lightning counts and (b) Gaussian lightning counts. Regression including outliers (shaded line); regression ignoring outliers (black line). Crosses pointed by arrows are the two extreme events that occurred over the season.

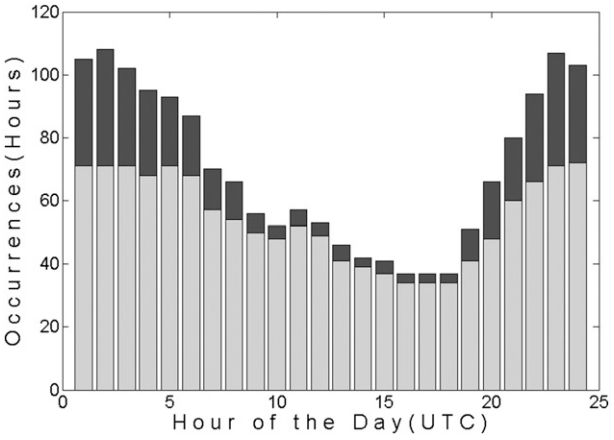

FIG. 9. Diurnal histogram (hourly) showing the number of hours in JJA 2005 with PEL (dark gray) and non-PEL (light gray).

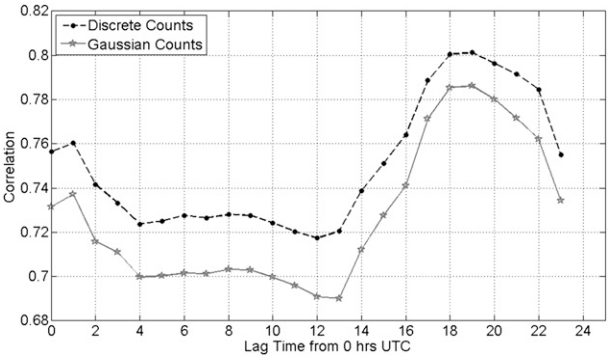

FIG. 10. Plot showing how the correlation (R) changes for several starting times of ''convective diurnal day'' time lag relative to UTC time. Derived from PEL and discrete counts (dashed line) and from Gaussian counts (solid line). Note that the highest values are around lag 18 and 19 h (1000 and 1100 LST), in concordance with the minimum precipitation in Fig. 9.

between lightning and precipitation. To minimize this problem, a temporally consistent ''convective day'' has been used in which the diurnal cycle of precipitation starts (the 0 h) at the hour with the lowest likelihood of precipitation (and also minimum likelihood of CG lightning). To demonstrate this behavior, the diurnal ''number of hours of occurrence'' for two conditions were analyzed—number of hours of precipitation with lightning (dark gray) and number of hours of precipitation with no lightning (shaded) results are plotted in an hourly stacked histogram (Fig. 9). Convective precipitation is more likely between hours 0000 and 0600 and between 2000 and 2400 UTC (1300–2300 LST), corresponding well with the total precipitation. The period with the least convective activity (and least hours of precipitation) is between 1600 and 1800 UTC (0900 and 1200 LST). There is a factor-of-two diurnal ''modulation'' of hours with precipitation. Interestingly, the diurnal modulation of hours with precipitation related to lightning varies by nearly a factor of 10. Comparing the results shown in Figs. 7 and 9, we see that more than half of the precipitation in the domain is associated with lightning, and it occurs in less than 1/3 of the total number of hours with precipitation. While 10 h per day of convective activity seems excessive for the Southwest, it should be noted that the domain covers ~160 km from east to west and considers geographic areas with slightly different timing in diurnal maximum in convection. Overall this result agrees with studies presented by Balling and Brazel (1987), Johnson et al. (2010), and Li et al. (2008).

Note that the convective fraction (fraction of precipitation hours associated with lightning) is extremely small between 0900 and 1700 UTC (0200–1000 LST), which is after most terrain-induced storms have propagated through the lowlands, and before solar heating can initiate deep convection. From the histogram, hours 1600, 1700, and 1800 UTC (0900, 1000, and 1100 LST) are the times of day that are least likely to have convective activity. To determine the most appropriate zero hour, R values were determined for convective days with different lag times with respect to the 0000 UTC. Figure 10 shows 2005 seasonal R obtained per each time lag. Based on this analysis, the diurnal seasonal time series was selected to start at lag hour 18 h later with respect to 0000 UTC (peak in correlation). This finding is also supported by Fig. 9 and agrees with the previous results of the diurnal cycle in the region that show a minimum convective activity in southern Arizona at about local noon (Balling and Brazel 1987; Johnson et al. 2010; Li et al. 2008). The daily accumulation scattergrams for the optimum lagged time are presented in Fig. 11 and the regression parameters are listed in Table 3; Fig. 11a relates PEL (volume) to lightning counts, and Fig. 11b relates PEL to the Gaussian integrated lightning counts. Correlation improved for both cases with respect to the R^2 presented in Fig. 8 (UTC day), with an increase 6% in the case of discrete lightning counts and 8% for Gaussian lightning counts.

e. *Specific event and storm evaluation*

One of the long-term aims of this work is to evaluate LPR over sufficiently short time and space scales to contribute to operational ''nowcasts'' of QPE, especially in regions with poor coverage of precipitation sensors. The LPR is likely to be different for air mass storms, multicellular storms, and MCSs, and may be a function of time of each storm type. In this initial work (and for this small spatial domain), it is not possible to show all the cases; however, we provide a case that illustrates most important behaviors. On 14 August 2005, an MCS affected a large portion of southern Arizona with precipitation falling over most of the test domain (Fig. 13).

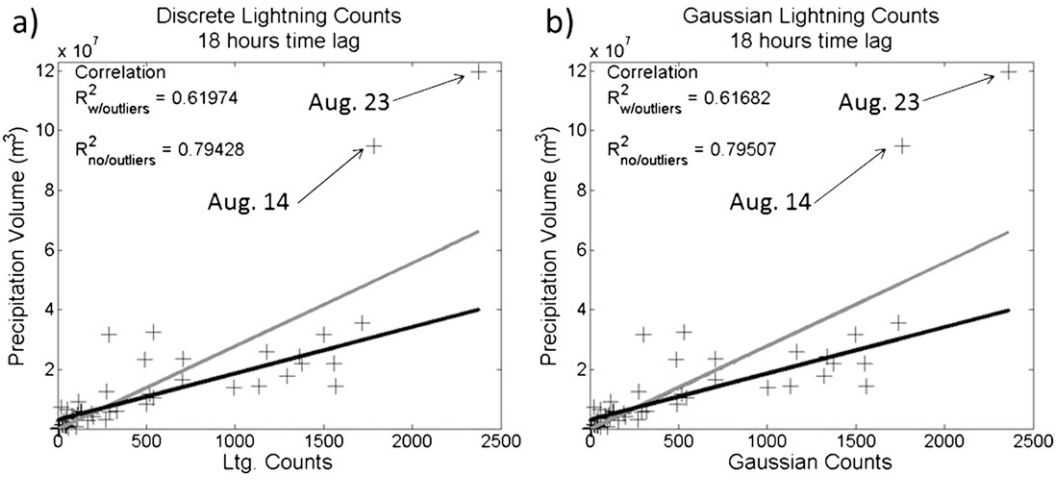

FIG. 11. As in Fig. 8 but for diurnal convective day (18 h, time lag).

At 1400 UTC there were two air mass thunderstorms over the southeast and northeast portions of the domain. During hours 1600, 1700, and 1800, these storms moved north and westward and organized, producing more than 40 mm h^{-1} of precipitation at some locations within the domain. The scattergrams in Fig. 12 show the hourly LPR for the event, considering the total precipitation and total lightning flash counts for the sensor-covered grids (similar to those in Fig. 11, but hourly time resolution). Note that R^2 values are all greater than 0.75, and that there is no clear nonlinearity in the LPR.

The panels in Fig. 13 show a sequence of images for this event. The first column shows the original total ST4 precipitation data, and the second column shows $\hat{P}$ from Gaussian integrated grids ($\hat{P}_{GC}$) using the regression in Table 4. A single yield (PVF) value was applied to all time steps. In this case, the y intercept is misleading, since the value in this regression corresponds to the whole sensor-covered domain; hence, it was divided by the area of the covered domain in order to apply to individual grids. Gaussian counts were preferred to describe this case because they expand the PEL domain and this has an impact on the number of data points when compared with precipitation. Finally, the third column in the figure shows the composite of both of these data—a first-order improved ''product'' that could be used to improve QPE. Specifically, $\hat{P}$ only replaces ST4 precipitation in nonsensor-covered grid cells.

We emphasize that our objective is to enhance QPE associated with convection in areas of poor radar and gauge coverage while not degrading the ST4 product. Therefore, if no lightning is recorded and the ST4 product shows some precipitation, the ST4 precipitation is not replaced with a zero value. Considering the nonsensor-covered cells, there is a noticeable difference between the original ST4 product and the combined ST4-lightning-derived QPE, especially in areas of complex terrain with radar beam blockage. This demonstrates the

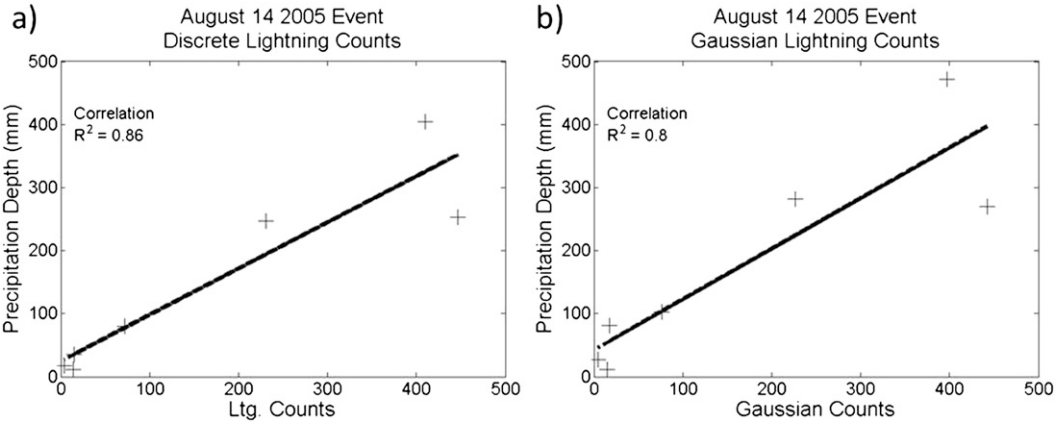

FIG. 12. Scattergrams for the August 2004 event. PEL vs (a) discrete lightning counts and (b) Gaussian counts.

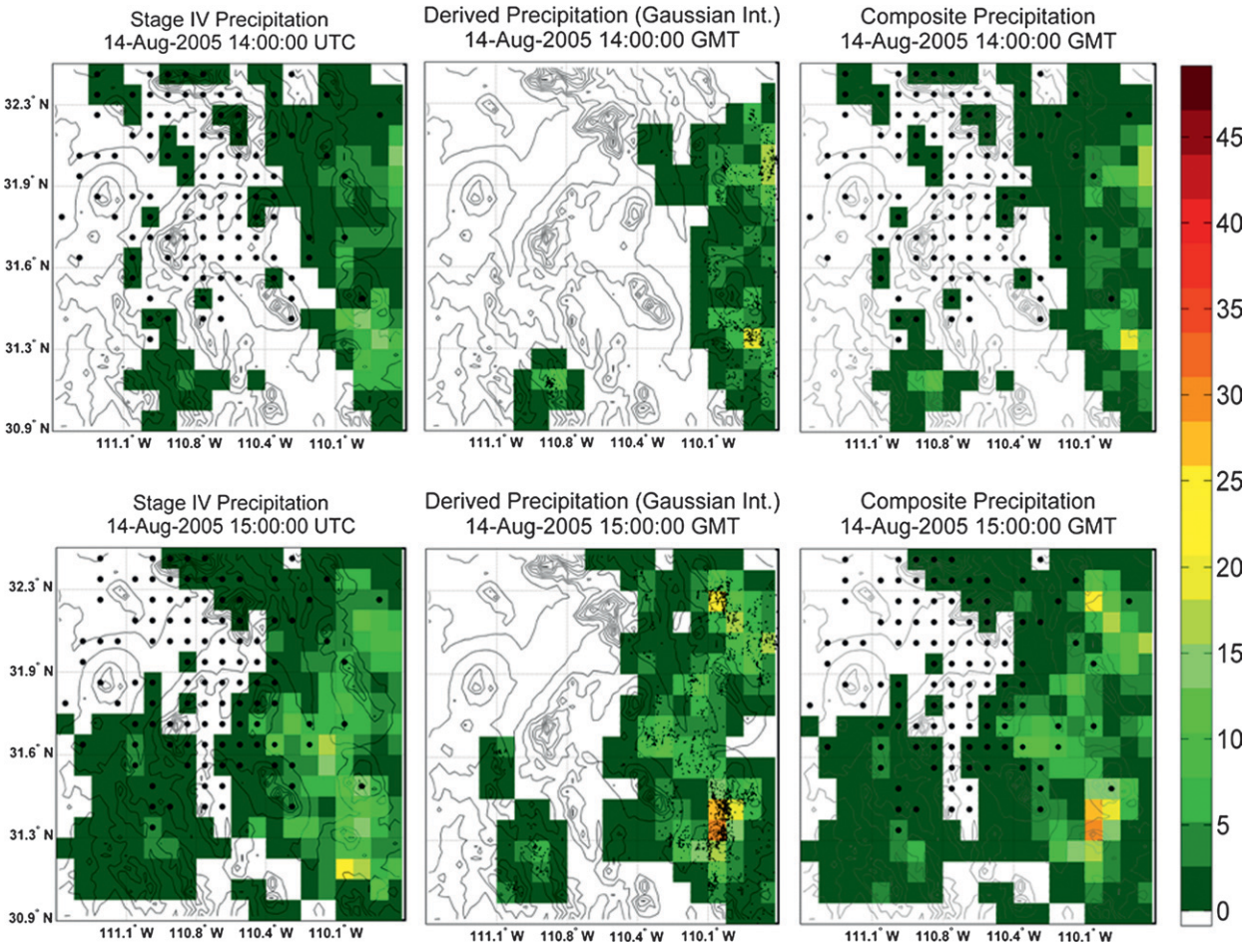

FIG. 13. (left) ST4 precipitation data (dots indicate covered grids), (center) derived precipitation from Gaussian counts (dots indicate CG lightning strikes), and (right) a composite of ST4 precipitation for covered grids and Gaussian counts derived precipitation for noncovered grids for 14 Aug event.

potential value of a lightning-enhanced, radar-derived precipitation product like $\hat{P}_{GC}$ (Fig. 13, second column) for improving the QPE in regions of intense convection. A good example occurs during hour 1500 (see Fig. 13), when the thunderstorms are starting to organize over the steep terrain of the Chiracahua Mountains in Cochise County (southeast part of the domain). In this region $\hat{P}_{GC}$ increased the QPE on the order of 10–20 mm h^{-1}, which is an amount that would be large enough to affect the issuance of flash flood advisories or warnings. The individual lightning strikes, as shown in the middle panel, clearly show the leading line of the convection. As the leading line moves through the Tucson metropolitan area during hours 1600 and 1700, the ST4 product shows lingering precipitation to the east associated with the trailing stratiform region of the organizing MCS, while $\hat{P}_{GC}$ shows less.

Even for deep convection, disagreement between the ST4 precipitation and $\hat{P}_{GC}$ is clear, especially in regions with poor sensor coverage, where even the manual quality control procedures used in ST4 algorithms would be inadequate to attain a good QPE (Lin and Mitchell 2005). We highlight the south-central region during hours 1600 and 1700, when ST4 is showing precipitation yields 20–40 mm h^{-1}, possibly because of brightband contamination of the radar beam, while $\hat{P}_{GC}$ does not show more than 10–15 mm h^{-1} for the same grids. At these hours, there is an additional discrepancy: at the center of the study region, there are a large number of flashes associated with the leading convective line of the MCS, but little ST4 precipitation. We suspect that this illustrates a weakness in the ST4 precipitation estimates. Though this area is considered by our criteria a "sensor covered," the closest rain gauges were between 10 and 16 km away from the heaviest $\hat{P}_{GC}$. There is just one radar tilt that covers two of these grids (<1000 m AGL), so clearly the ST4 estimate is in question. However, in the absence of independent measurements we cannot make a definitive interpretation about this.

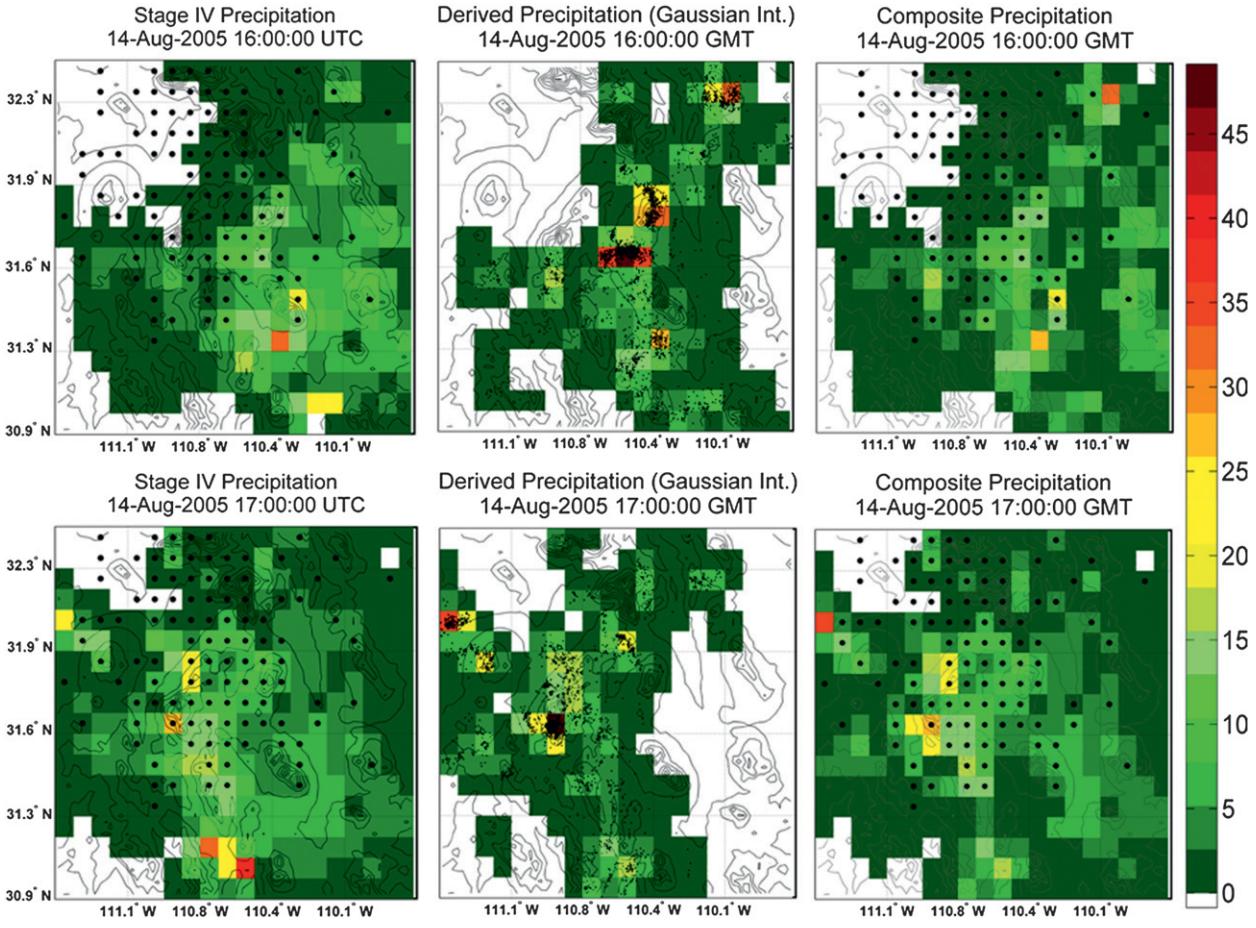

FIG. 13. (*Continued*)

During hour 1800 (Fig. 13) most of the organized convection was located in the northwest portion of the spatial domain where the storms were actively producing lightning. Hour 1800 was found to have the best agreement between PEL and $\hat{P}_{GC}$, as seen in Fig. 14. Finally at hour 2000, the event had left the domain and only stratiform precipitation remained in the region, with few lightning strikes.

Figure 14 shows the percentage of PEL (solely for covered grids) and correlation time series, using the Gaussian counts. The time evolution of the propagating, organized MCS is loosely represented by the time series. Prior to hour 1400, before the thunderstorms develop and produce substantial rainfall over the Chiricahua Mountains, there is virtually no precipitation explained by lightning and correlation is obviously zero. When deep convection develops by the next 2 h PEL rapidly increases up to approximately 60%; R^2 reaches its highest value at hour 1800 and coincides with the time when PEL is high. After the event passes through the domain and only stratiform precipitation is present, the PEL percentage then decreases gradually over the next few hours. Even with the relatively coarse temporal (hourly) information used in this study, there is a clear deficiency in the ability of lightning (as employed in this study) to provide QPE information in situations where a substantial portion of the domain is covered by stratiform precipitation.

Overall, areas that had a high lightning density generally were associated with high precipitation rates (typically >20 mm h^{-1}), but the converse did not necessary occur. Moderate precipitation rates (2.5–10 mm h^{-1}) were generally in close proximity to lightning. ST4 estimates of precipitation in poor coverage regions can have very high precipitation rates (~35–45 mm h^{-1}) with no lightning occurrence (Fig. 13 southern grids at 1700 UTC), and these measurements are quite suspect (perhaps because of radar reflectivity from altitudes above 2 km AGL). Such high precipitation rates did not occur in the covered region unless they were associated with lightning similar to the seasonal case in section 4a. The highest PEL (>60%) occurred during the periods when deep convection was present, as did the highest correlation values. Both PEL and

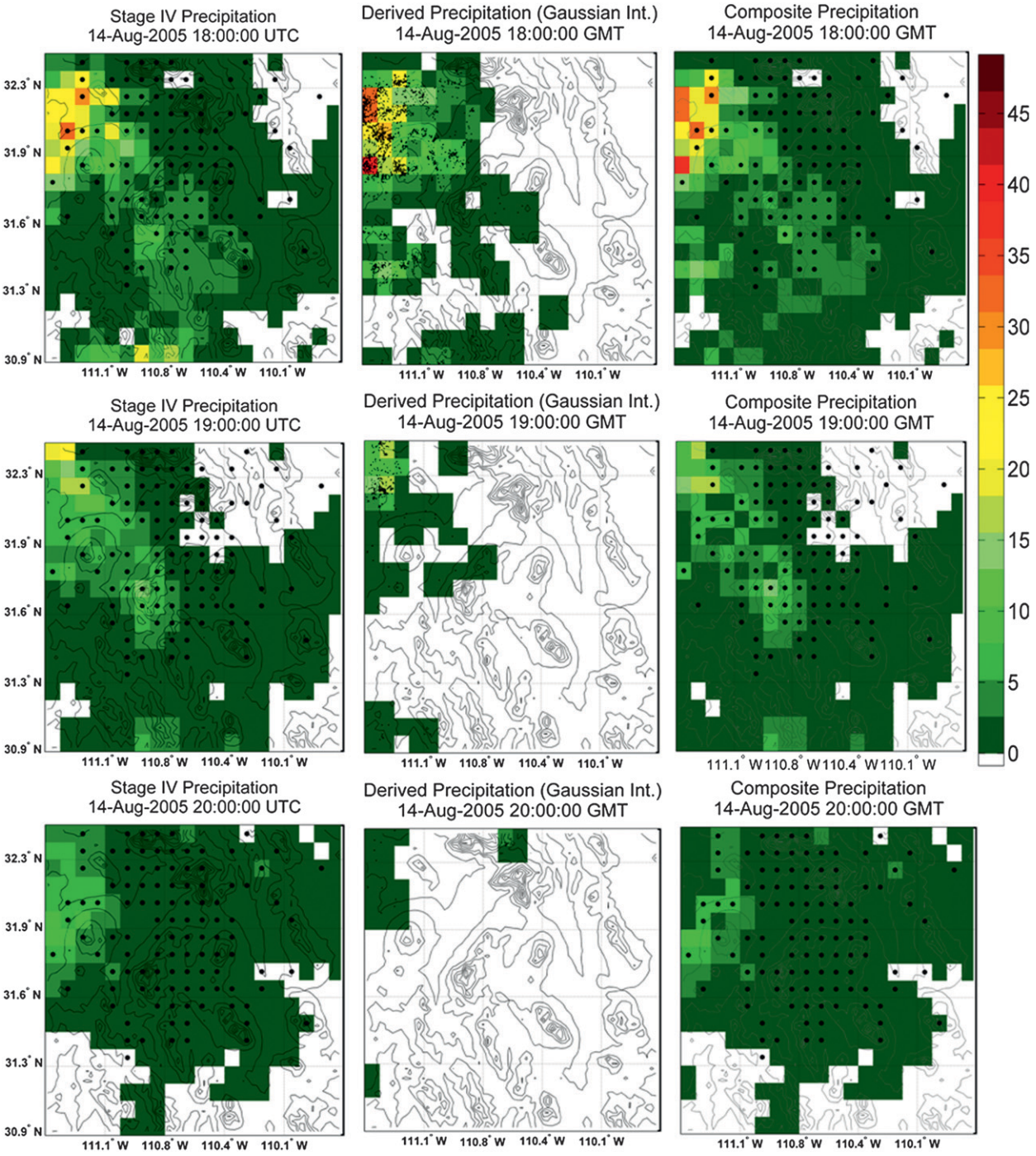

FIG. 13. (*Continued*)

correlation were low when mostly stratiform precipitation occurred.

5. Discussion

ST4 is considered one of the best available short-term gridded precipitation datasets for the contiguous United States because of its quality control; however, the quality of this dataset decreases in areas with poor sensor (radar and gauge) coverage. Within the mountainous domain considered in this study, there are areas with poor gauge coverage and complete radar beam blockage. Since QPE depends on such observations, any analysis of the LPR in these regions will be

TABLE 3. Regression parameters from Fig. 11.

Case (a) precipitation volume vs lightning counts					
m		*y* intercept			
m^3 flash^{-1}	mm flash^{-1}	m^3	mm	R	R^2
14 600	0.22	2 431 100	38.0	0.81	0.67
Case (b) precipitation volume vs integrated Gaussian					
15 600	0.24	3 084 600	48.2	0.79	0.63

TABLE 4. Regression parameters from Fig. 12.

Case (a) precipitation depth vs lightning counts			
m (mm flash^{-1})	*y* intercept (mm)	R	R^2
0.73	25.20	0.93	0.86
Case (b) precipitation depth vs integrated Gaussian			
0.80	42.77	0.89	0.80

adversely affected if areas with poor coverage are included in the analysis. A rigorous assessment of the in situ gauges and radar coverage is required to determine the ''good'' data points that can be used in constructing a regression. The resulting precipitation yield (mm/flash or m^3/flash) for the region under study was of the same order as that obtained by Battan (1965) and Petersen and Rutledge (1998), and may well be characteristic of the North American monsoon region as a whole.

There is no simple perfect criterion to differentiate between convective and stratiform precipitation. In this study, we have proposed a method for using counts of CG lightning to estimate precipitation (assuming that most convective precipitation is related to CG lightning) where we have demonstrated that the ''precipitation explained by lightning'' (PEL) can be used to complement other criteria (like precipitation rate) for classifying convective precipitation, especially in an operational setting.

The use of spatially smoothed data (Gaussian counts) instead of lightning counts impacts the fraction of PEL as seen for the JJA 2005 season where the percentage change from 52% using discrete counts to 67%, indicating that much of the precipitation is in close proximity with lightning discharges (specifically, within 2σ; i.e., 5 km). At hourly time resolution, the increase in PEL resulting from Gaussian smoothing contributes positively in two ways: 1) by augmenting the number of data points in the linear regression for precipitation estimation, and hence, improving statistical significance and correlation; and 2) by allowing better tracking of convective events, which includes times and locations that are otherwise neglected when only discrete counts are utilized. This last result will be more important as the spatial and temporal resolution is increased in future studies. The Gaussian smoothing tended to slightly decrease R^2 values, likely because of the large (8×8 km^2) grid size employed in this analysis. Both the ST4 precipitation and PEL exhibit strong diurnal modulation (2 times for total precipitation and 10 times for PEL—deep convection). This, in turn, impacts daily analysis and makes necessary the concept of a ''convective'' day, which should be employed in place of solar or LST days in regions with complex terrain.

Our findings clearly show that lightning-derived precipitation can substantially contribute to the estimation of warm season precipitation in southern Arizona, especially in regions that have no rain gauge coverage and poor radar coverage. We expect that the same would be true throughout the intermountain west, because the entire region can experience topographically forced monsoon thunderstorms (at least during part of the summer). With higher time resolution, QPE employing lightning-derived precipitation could improve our ability to provide flood advisories, as well as improve our physical understanding of the hydroclimatology associated with the North American monsoon.

Future work will expand this research along three lines. Convective QPE can be further improved when using radar-derived precipitation products with spatiotemporal resolution comparable to the NLDN, such as the National Mosaic and Multisensor QPE (NMQ). This will provide better spatial localization of convective cells and allow for storm tracking, thereby improving PEL estimation. Eventually we plan to use a Kalman filtering approach to derive a time-evolving lightning–precipitation relationship. This analysis will consider precipitation data that are more spatiotemporally resolved and, thus, better suited to characterizing monsoon thunderstorms.

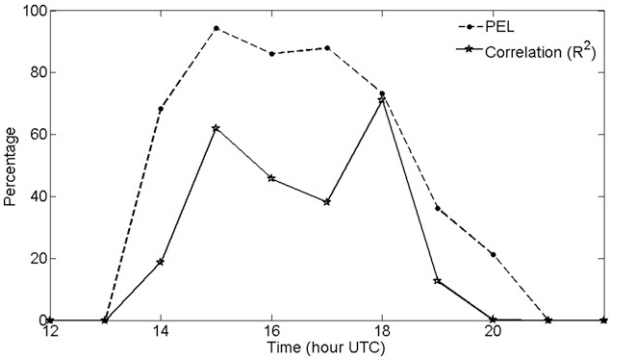

FIG. 14. Time series for 14 Aug event: PEL percentage and R^2 between PEL and CG lightning, both using Gaussian counts.

Acknowledgments. Support of this work was provided by the CONACYT Fellowship 187242, The University of Arizona through a Graduate Incentives for Growth Award (GIGA) Fellowship, the University of Sonora, and Vaisala Inc.

REFERENCES

Adams, D. K., and A. C. Comrie, 1997: The North American monsoon. *Bull. Amer. Meteor. Soc.,* **78,** 2197–2213.

——, and E. P. Souza, 2009: CAPE and convective events over the Southwest during the North American monsoon. *Mon. Wea. Rev.,* **137,** 83–98.

Anagnostou, E., 2004: Overview of overland satellite rainfall estimation for hydro-meteorological applications. *Surv. Geophys.,* **25,** 511–537.

Baker, M. B., H. J. Christian, and J. Latham, 1995: A computational study of the relationships linking lightning frequency and other thundercloud parameters. *Quart. J. Roy. Meteor. Soc.,* **121,** 1525–1548.

Balling, R. C., Jr., and S. W. Brazel, 1987: Diurnal variations in Arizona monsoon precipitation frequencies. *Mon. Wea. Rev.,* **115,** 342–346.

Battan, L. J., 1965: Some factors governing precipitation and lightning from convective clouds. *J. Atmos. Sci.,* **22,** 79–85.

Becker, J., and E. H. Berbery, 2008: The diurnal cycle of precipitation over the North American monsoon region during the NAME 2004 field campaign. *J. Climate,* **21,** 771–787.

Biagi, C. J., K. L. Cummins, K. E. Kehoe, and E. P. Krider, 2007: National Lightning Detection Network (NLDN) performance in southern Arizona, Texas, and Oklahoma in 2003–2004. *J. Geophys. Res.,* **112,** D05208, doi:10.1029/2006JD007341.

Castro, C. L., R. A. Pielke Sr., and J. O. Adegoke, 2007: Investigation of the summer climate of the contiguous United States and Mexico using the Regional Atmospheric Modeling System (RAMS). Part I: Model climatology (1950–2002). *J. Climate,* **20,** 3844–3865.

Cheze, J. L., and H. Sauvageot, 1997: Area-average rainfall and lightning activity. *J. Geophys. Res.,* **102** (D2), 1707–1705.

Crosson, W. L., C. E. Duchon, R. Raghavan, and S. J. Goodman, 1996: Assessment of rainfall estimates using a standard *Z–R* relationship and the probability matching method applied to composite radar data in central Florida. *J. Appl. Meteor.,* **35,** 1203–1219.

Cummins, K. L., and M. J. Murphy, 2009: An overview of lightning locating systems: History, techniques, and data uses, with an in-depth look at the U.S. NLDN. *IEEE Trans. Electromagn. Compat.,* **51,** 499–518.

——, ——, E. A. Bardo, W. L. Hiscox, R. B. Pyle, and A. E. Pifer, 1998: A combined TOA/MDF technology upgrade of the U.S. National Lightning Detection Network. *J. Geophys. Res.,* **103** (D8), 9035–9044.

Daly, C., R. P. Neilson, and D. L. Phillips, 1994: A statistical-topographic model for mapping climatological precipitation over mountainous terrain. *J. Appl. Meteor.,* **33,** 140–158.

Douglas, M. W., R. A. Maddox, K. Howard, and S. Reyes, 1993: The Mexican monsoon. *J. Climate,* **6,** 1665–1677.

Fher, T., N. Dotzek, and H. Holler, 2005: Comparison of lightning activity and radar-retrieved microphysical properties in EULINOX storms. *Atmos. Res.,* **76,** 167–189.

Foote, G. B., 1996: A Z–R relation for mountain thunderstorms. *J. Appl. Meteor.,* **5,** 229–231.

Fulton, R. A., 1999: Sensitivity of WSR-88D rainfall estimates to the rain-rate threshold and rain gauge adjustment: A flash flood case study. *Wea. Forecasting,* **14,** 604–624.

——, J. P. Breidenbach, D. J. Seo, and D. A. Miller, 1998: The WSR-88D rainfall algorithm. *Wea. Forecasting,* **13,** 377–395.

Grecu, M., and W. F. Krajewski, 2000: A large-sample investigation of statistical procedures for radar-based short-term quantitative precipitation forecasting. *J. Hydrol.,* **239,** 69–84.

Gungle, B., and E. P. Krider, 2006: Cloud-to-ground lightning and surface rainfall in warm-season Florida thunderstorms. *J. Geophys. Res.,* **111,** D19203, doi:10.1029/2005JD006802.

Houze, R. A., Jr., B. F. Smull, and P. Dodge, 1990: Mesoscale organization of springtime rainstorms in Oklahoma. *Mon. Wea. Rev.,* **118,** 613–654.

Johnson, R. H., P. E. Ciesielski, T. S. L'Ecuyer, and A. J. Newman, 2010: Diurnal cycle of convection during the 2004 North American Monsoon Experiment. *J. Climate,* **23,** 1060–1078.

Krajewski, W. F., and J. A. Smith, 2002: Radar hydrology: Rainfall estimation. *Adv. Water Resour.,* **25,** 1387–1394.

Kursinski, A., and X. Zeng, 2006: Areal estimation of intensity and frequency of summertime precipitation over a mid-latitude region. *Geophys. Res. Lett.,* **33,** L22401, doi:10.1029/2006GL027393.

Latham, J., A. M. Blyth, H. J. Christian Jr., W. Deierling, and A. M. Gadian, 2004: Determination of precipitation rates and yields from lightning measurements. *J. Hydrol.,* **288,** 13–19.

——, W. A. Petersen, W. Dejerling, and H. J. Christian, 2007: Field identification of a unique globally dominant mechanism of thunderstorm electrification. *Quart. J. Roy. Meteor. Soc.,* **133,** 1453–1457, doi:10.1002/qj.133.

Lhermitte, R., and P. R. Krehbiel, 1979: Doppler radar and radio observations of thunderstorms. *IEEE Trans. Geosci. Electron.,* **17,** 162–171.

Li, J., S. Sorooshian, W. Higgins, X. Gao, B. Imam, and K. Hsu, 2008: Influence of spatial resolution on diurnal variability during the North American monsoon. *J. Climate,* **21,** 3967–3988.

Lin, Y., and K. E. Mitchell, 2005: The NCEP stage II/IV hourly precipitation analyses: Development and applications. Preprints, *19th Conf. on Hydrology,* San Diego, CA, Amer. Meteor. Soc., 1.2. [Available online at https://ams.confex.com/ams/Annual2005/techprogram/paper_83847.htm.]

MacGorman, D. R., D. W. Burgess, V. Mazur, W. D. Rust, W. L. Taylor, and B. C. Johnson, 1989: Lightning rates relative to tornadic storm evolution on 22 May 1981. *J. Atmos. Sci.,* **46,** 221–250.

——, and Coauthors, 2008: TELEX: The Thunderstorm Electrification and Lightning Experiment. *Bull. Amer. Meteor. Soc.,* **89,** 997–1013.

Maddox, R. A., D. M. McCollum, and K. W. Howard, 1995: Large-scale patterns associated with severe summertime thunderstorms over central Arizona. *Wea. Forecasting,* **10,** 763–778.

——, J. Zhang, J. Gourley, and K. Howard, 2002: Weather radar coverage over the contiguous United States. *Wea. Forecasting,* **17,** 927–934.

Mansell, E. R., D. R. MacGorman, C. L. Ziegler, and J. M. Straka, 2005: Charge structure in a simulated multicell thunderstorm. *J. Geophys. Res.,* **110,** D12101, doi:10.1029/2004JD005287.

Morin, E., R. Maddox, D. Goodrich, and S. Sorooshian, 2005: Radar *Z–R* relationship for summer monsoon storms in Arizona. *Wea. Forecasting,* **20,** 672–679.

Petersen, W. A., and S. A. Rutledge, 1998: On the relationship between cloud-to-ground lightning and convective rainfall. *J. Geophys. Res.,* **103** (D12), 14 025–14 040.

Piepgrass, M. V., E. P. Krider, and C. B. Moore, 1982: Lightning and durface rainfall during Florida thunderstorms. *J. Geophys. Res.,* **87,** 11193–11201.

Reap, R. M., and D. R. MacGorman, 1989: Cloud-to-ground lightning: Climatological characteristics and relationships to model fields, radar observations, and severe local storms. *Mon. Wea. Rev.,* **117,** 518–525.

Rutledge, S. A., and D. R. MacGorman, 1988: Cloud-to-ground lightning activity in the 10–11 June 1985 mesoscale convective system observed during the Oklahoma–Kansas PRE-STORM project. *Mon. Wea. Rev.,* **116,** 1393–1408.

Saylor, J. R., C. W. Ulbrich, J. W. Ballentine, and J. L. Lapp, 2005: The correlation between lightning and DSD parameters. *IEEE Trans. Geosci. Remote Sens.,* **43,** 1806–1815.

Smith, J. A., and W. F. Krajewski, 1993: A modeling of rainfall rate-reflectivity relationships. *Water Resour. Res.,* **29,** 2505–2514.

Smith, W. P., and R. L. Gall, 1989: Tropical squall lines of the Arizona monsoon. *Mon. Wea. Rev.,* **117,** 1553–1569.

Sorooshian, S., R. Lawford, P. Try, W. Rossow, J. Roads, J. Polcher, G. Sommeria, and R. Schiffer, 2005: Water energy cycles: Investigating the links. *WMO Bull.,* **54,** 58–60.

Soula, S., and S. Chauzy, 2001: Some aspects of the correlation between lightning and rain activities in thunderstorms. *J. Atmos. Res.,* **56,** 355–373.

Stall, C., K. Cummins, E. P. Krider, and J. Cramer, 2009: Detecting multiple ground contacts in cloud-to-ground lightning flashes. *J. Atmos. Oceanic Technol.,* **26,** 2392–2402.

Stellman, K. M., H. E. Fuelberg, R. Garza, and M. Mullusky, 2001: An examination of radar and rain gauge-derived mean areal precipitation over Georgia watersheds. *Wea. Forecasting,* **16,** 133–144.

Takahashi, T., 1990: Near absence of lightning in torrential rainfall producing Micronesian thunderstorms. *Geophys. Res. Lett.,* **17,** 2381–2384.

Tapia, A., J. A. Smith, and M. Dixon, 1998: Estimation of convective rainfall from lightning observations. *J. Appl. Meteor.,* **37,** 1497–1509.

Todd, M. C., C. Kidd, D. Kniveton, and T. J. Bellerby, 2001: A combined satellite infrared and passive microwave technique for estimation of small-scale rainfall. *J. Atmos. Oceanic Technol.,* **18,** 742–755.

Wiens, K. C., S. A. Rutledge, and S. A. Tessendorf, 2005: The 20 June 2000 supercell observed during STEPS. Part II: Lightning and charge structure. *J. Atmos. Sci.,* **62,** 4151–4177.

Xie, P., and P. A. Arkin, 1995: An intercomparison of gauge observations and satellite estimates of monthly precipitation. *J. Appl. Meteor.,* **34,** 1143–1160.

Zehnder, J., J. Hu, and A. Radzan, 2009: Evolution of the vertical thermodynamic profile during the transition from shallow to deep convection during CuPIDO 2006. *Mon. Wea. Rev.,* **137,** 937–953.